FLEXIBLE ZNO THIN FILM ACOUSTIC WAVE DEVICE FOR GAS FLOW RATE MEASUREMENT

Qian Zhang[a], Yong Wang[a,b], Ran Tao[b,c], Hamdi Torun[b], Jin Xie[a,*], Yifan Li[b], Chen Fu[c], Jingting Luo[c], Qiang Wu[b], Wai Pang Ng[b], Richard Binns[b], Yong Qing Fu[b,*]

[a] The State Key Laboratory of Fluid Power and Mechatronic Systems, Zhejiang University, Hangzhou 310027, China

[b] Faculty of Engineering and Environment, University of Northumbria, Newcastle upon Tyne NE1 8ST, UK

[c] Shenzhen Key Laboratory of Advanced Thin Films and Applications, College of Physics and Optoelectronic Engineering, Shenzhen University 518060, China

* Corresponding authors: xiejin@zju.edu.cn; Richard.fu@northumbria.ac.uk;

Abstract

In this work, ZnO/Al thin film based flexible acoustic wave devices are demonstrated for their applications in gas flow rate measurements based on the changes in temperature of the devices. A good sensitivity of gas flow rate can be achieved, mainly because thin film based device has a large temperature coefficient of frequency of ~280 ppm/K, owing to the large coefficient of thermal expansion of aluminum foil. A heat source is used to enhance the sensitivity of the thin film device by introducing a temperature offset. The flexible acoustic wave device shows a high sensitivity, fast response times, and a good repeatability for measurement of the flow rate of nitrogen. When the flexible acoustic wave device is bent and attached onto the inner wall of a pipe, the device exhibits good performance for monitoring the gas flow rate, demonstrating its applications of flow rate measurement on curved or randomly shaped surfaces.

Keywords: surface acoustic wave, flexible device, gas flow rate measurements

1. Introduction

Flexible electronics have rapidly emerged for wearable device applications in recent years owing to their unique advantages to their rigid counterparts. Various flexible devices and technologies have been reported as sensors [1], [2], electrodes [3], transistors [4], printed electronics [5], and nanogenerators [6]. As a member of flexible electronics, flexible acoustic wave devices have advantages of high sensitivity, good reliability, low power consumption, and easy integration with digital circuits [7]. For example, Xuan et al. reported flexible Lamb wave humidity sensors fabricated by depositing ZnO thin films on polyimide substrates with a sensitivity of 145.83 ppm/%RH (at humidity 85%RH) [8]. Chen et al. reported ZnO thin film based bendable and transparent surface acoustic wave (SAW) strain sensors fabricated on flexible glass substrates with excellent linearity and a sensitivity of ~34 Hz/με [9]. Xu et al. presented dual-mode (Rayleigh mode and thickness shear mode) SAW strain sensors based on flexible 128°Y-cut lithium niobate thin films [10]. Recently, we have developed flexible Lamb wave devices by depositing ZnO thin film on commercially available and low-cost aluminum foils, which have demonstrated excellent performance in temperature sensing [11], ultraviolet light sensing [12] and microfluidics [13, 14], and lab-on-a-chip [15].

Flow rate measurements are critical for numerous applications, such as biomedical flow control, environmental and industrial flow monitoring, aerospace, automotive system, respiratory monitoring [16]–[19]. Various types of flow meters based on microelectromechanical systems (MEMS) technology have been developed based on different transduction mechanisms such as thermal [20], piezoresistive [21], piezoelectric [22], ultrasonic [23] and capacitive [24]. For example, Joshi developed a 128°Y-cut lithium niobate based SAW flow sensor which shows a frequency shift larger than 142 kHz with an initial temperature offset of about 55 °C and a flow rate of 1 liters-per-minute (LPM) [25]. Zhou et al. developed a Lamb wave microsensor with AlN/Si structure and investigated the interaction between gas flow and acoustic waves [26]. Compared with the conventional flow meters, MEMS based flow meters show advantages of small size, less interference to the flow field, high sensitivity, low power consumption and low cost.

Flow rates can be indirectly measured by precisely detecting temperature of SAW or Lamb wave devices. According to Newton's Law, the heat transfer rate is directly proportional to the temperature difference. According to thermal boundary layer theory [27], the temperature difference between the solid and gas is mainly concentrated in a thin layer on the solid surface, i.e., a thermal boundary layer, which results in the most thermal resistance of convective heat transfer. When the temperature of the acoustic wave device is higher than the airflow, the larger the airflow rate, the thinner the boundary layer, the larger the temperature gradient in the boundary layer, the larger the heat exchange rate, and the lower the temperature of the acoustic wave device in the equilibrium state. The initial temperature offset can be provided by a heat source, which introduces a temperature difference between the acoustic wave device and airflow. When the airflow passes, heat is taken away and temperature of the acoustic wave device decreases. The change in temperature of the substrate causes a shift in resonant frequency, which depends on the temperature coefficient of frequency (TCF) of the acoustic wave device. The sensitivity of acoustic wave device increases with the TCF, so a large TCF is desirable for a highly sensitive thermal flowmeter. Owing to the large value of TCF for the ZnO/Al flexible Lamb wave devices [11], it is possible to achieve a high sensitivity in flow rate measurements. In this paper, constant power heat source (CPHS) and constant temperature heat source (CTHS) are respectively employed to investigate the frequency response of the flexible acoustic wave device. The CPHS mode shows high sensitivity while the CTHS mode shows fast response. In other aspects, the CPHS mode is simple to use, because only a constant power supply is needed, but with a drawback of slow response. The CTHS mode significantly decreases the response time. However, a complicated feedback control system is required, which may introduce additional noise due to the fluctuations of the temperature of the heat source.

This paper is an extended version of work published in IEEE MEMS Conference 2020 [28]. We extend our previous work by adding the following new results: theoretical model analysis, experiments with CPHS mode, comparison between CPHS and CTHS modes, analysis of hysteresis characteristic, and comparison between our flexible Lamb wave flow senor and other reported rigid SAW flow sensors in literature. Using aluminum foil as the substrate, the acoustic wave device is flexible and capable to conform to curved surfaces. This feature is advantageous for the measurement of flow rates at important and application-specific locations, such as duct walls, surfaces of aircrafts and vehicles, and building walls. In addition, the device has the merits of being small and light, and having less interference with the original flow field.

2. Modeling

2.1 Equivalent circuit model

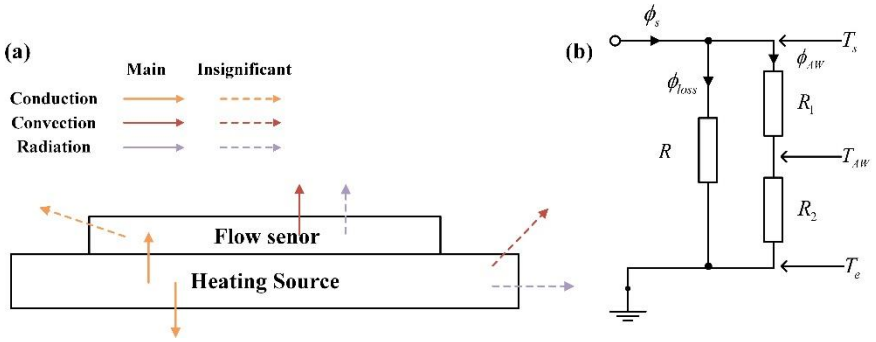

Fig. 1. (a) Schematic diagram of thermal equilibrium analysis. (b) The equivalent circuit model in equilibrium state.

As illustrated in Fig. 1a, there are three common ways of heat transfer: conduction, convection, and radiation. According to the Supporting Information, the heat transfer via radiation can be ignored because it is much less than the heat loss caused by conduction and convection. Conduction and convection effects are expressed by:

$$\text{conduction, } \phi = A\lambda\, d(T_h - T_l)/dx \tag{1}$$

$$\text{convection, } \phi = Ah(T_h - T_l) \tag{2}$$

where ϕ = heat flow, A = surface area of the device, λ = thermal conductivity, T_h = higher temperature, T_l = lower temperature, x = the distance parallel to the direction of heat flow, h = heat transfer coefficient. In Fig. 1a, the dotted and solid arrows indicate the insignificant and the main thermal paths, respectively. For simplicity, we only consider the solid arrows. Moreover, we assume that thermal conductivity λ and convective heat transfer coefficient h do not change with temperature, and thus we can obtain the equivalent circuit model as shown in Fig. 1b. R, R_1, and R_2 are the equivalent thermal resistances between the heat source and environment, between

the heat source and the surface of the flexible device, and between the surface of the flexible device and environment, respectively. The three equivalent thermal resistances are defined as:

$$R = \frac{x}{A\lambda},\ R_1 = \frac{x_1}{A\lambda_1},\ R_2 = \frac{1}{Ah} \tag{3}$$

where x_1 = thickness of the flexible device, λ_1 = thermal conductivity of the flexible device, x and λ are the equivalent values of a thermal resistance network. Due to the heat dissipation from the heat source is complicated, R is actually a thermal resistance network formed by multiple thermal resistances in series and parallel.

2.2 Steady state response

Based on the Supporting Information, we can obtain the following equation:

$$\frac{dT_{AW}}{dh} = -\frac{R+R_1}{R+R_1+R_2} \cdot \frac{AR_2^2}{R_1+R_2}(T_s - T_e) \tag{4}$$

where T_s = heat source temperature, T_e = ambient temperature, T_{AW} = acoustic wave device temperature. This equation can be regarded as the sensitivity formula in the case of using a CPHS. Similarly, the sensitivity formula for the case of using a CTHS is:

$$\frac{dT_{AW}}{dh} = -\frac{R_1}{R_1+R_2} \cdot \frac{AR_2^2}{R_1+R_2}(T_s - T_e) \tag{5}$$

Equations (4) and (5) reveal that the sensitivity of a system using the CTHS is lower than that of a system using the CPHS under equal initial temperature offset values. In the extreme case of $R_1 >> R_2$, the two sensitivities are approximately equal. The TCF is defined as:

$$TCF = \frac{\Delta f}{f_0 \Delta T_{AW}} \tag{6}$$

where Δf = resonant frequency shift, f_0 = initial resonant frequency and ΔT_{AW} = change in temperature of the acoustic wave device.

2.3 Transient response

The transient temperature response can be expressed as [25]:

$$mC\frac{dT}{dt} = \phi_{AW} - AhT \tag{7}$$

where ϕ_{AW} is the heat flow shown in Fig. 1b, m and C are the mass and specific heat of the acoustic wave device, respectively, T is temperature change of the acoustic wave device and t is time. The transient temperature response with the CPHS is:

$$T = \frac{R\phi_s/(R+R_1)}{Ah+1/(R+R_1)}\left(1 - e^{-\frac{t}{\tau_1}}\right) \tag{8}$$

where $\tau_1 = \frac{mC}{Ah+1/(R+R_1)}$ and ϕ_s = total heat flow out of the heat source as shown in Fig. 1b. Similarly, the transient temperature response with the CTHS is:

$$T = \frac{T_s - T_e}{AhR_1+1}\left(1 - e^{-\frac{t}{\tau_2}}\right) \tag{9}$$

where $\tau_2 = \frac{mC}{Ah+1/R_1}$. It is obvious that $\tau_1 > \tau_2$, and the transient frequency shift and time have an exponential relationship. The response of the system with the CTHS is faster than that with the CPHS.

3. Fabrication of acoustic wave device

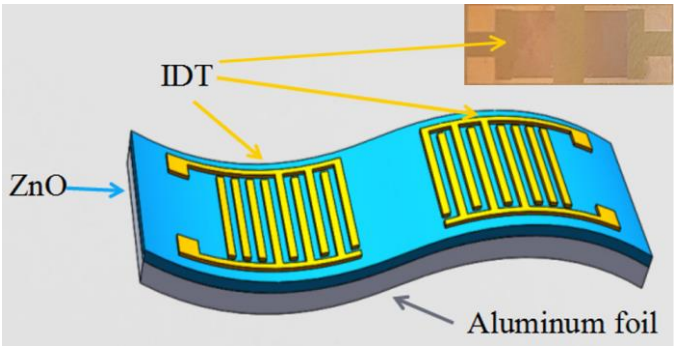

Fig. 2. Schematic diagram and optical image (inset) of the flexible acoustic wave device.

For fabrication of the flexible acoustic wave device, a 5-μm-thick ZnO film was deposited on a commercially available aluminum foil with a thickness of ~50 μm, using a DC sputter system (Nordiko 3750). Then a layer of Cr/Au (with thicknesses of 20/100 nm) was deposited and patterned to form the interdigital transducers (IDTs) using a standard lift-off process. The wavelength of the IDT is 100 μm. The schematic diagram and optical images of the flexible device are shown in Fig. 2. The detailed fabrication process was described in our previous work [13,29,30].

4. Experimental setup

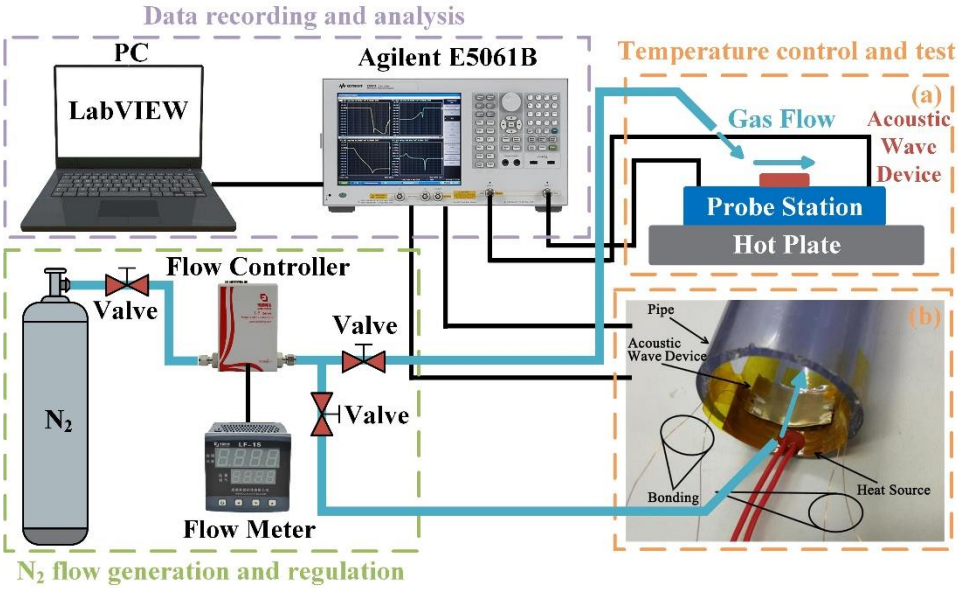

Fig. 3. Experimental setup. (a)The flat acoustic wave device is fixed on a probe station heated by CTHS. (b) The curved acoustic wave device and CPHS are fixed together in a pipe.

Fig. 3 shows the experimental setup for flow rate measurement with a CTHS in (a) or a CPHS in (b). As shown in Fig. 3a, the flexible device is fixed on an aluminum probe station, and then connected to a vector network analyzer (Agilent E5061B) through coaxial wires. The probe station is placed on top of a hot plate. The probe station effectively acts as a heat sink as it has a high thermal conductivity and a large heat capacity. Therefore, the surface temperature of the probe station can be kept practically constant, and interference caused by temperature fluctuations can be minimized. Compressed nitrogen gas is used as the gas source, and a flow controller and a flowmeter are used to control and measure the flow rate, respectively. Polyurethane (PU) gas pipes with an inner diameter of 4 mm is used for connection. The end of the air pipe is fixed by a clamp on an iron stand, and the distance from the acoustic wave device is ~5 mm. The angle between the axis at the end of the pipe and the normal of the acoustic wave device is ~45°.

Fig. 3b shows the experimental setup in which the CTHS in Fig. 3a is replaced with a flexible CPHS. Both the CPHS and acoustic wave device are attached onto the inner wall of a polyvinyl chloride (PVC) pipe. The CPHS is an electric resistance heating film (with the rated voltage/power of 12V/20W), and its outer insulation layer is polyimide (PI). The heating power can be controlled by changing the input voltage.

In the experiment, the flow field is a multi-dimensional and complex variable, and is affected by many factors, including the relative position and angle between the PU gas pipe outlet and the acoustic wave device, the PU gas pipe diameter, the gas flow velocity at the pipe outlet, and the curved shape of the device surface. The flow field is uniquely defined by four parameters, including the relative position and angle between the end of the PU gas pipe and the device, the diameter of the PU gas pipe, and the flow rate of the gas in the pipe. Once these four parameters are specified, the flow field can be defined. Therefore, we keep the first three parameters unchanged and only change the flow rate. According to simulation, the flow rate of gas in the pipe is approximately proportional to the average velocity near the surface of the acoustic wave device. Based on the previous analysis, the flow field near the device can be determined and calculated as a function of the flow rate in the pipe. For a simple model such as the one in this experiment, the simulated flow field differs slightly from the actual flow field.

5. Results and discussion

5.1 Characterization and measurements

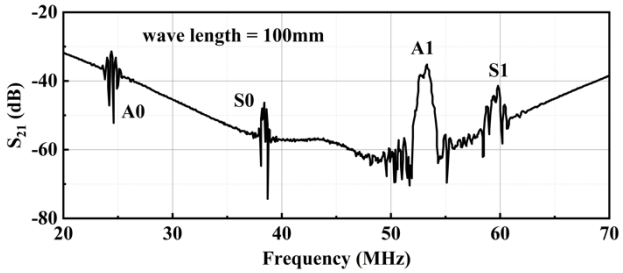

Fig. 4. Transmission spectrum of the flexible acoustic wave device.

Fig. 4 shows the transmission spectrum (S21) of the flexible acoustic wave device with multiple Lamb wave modes of A0, S0, A1 and S1. Simulations and discussion including these modes for these ZnO/Al acoustic wave devices have been reported in our previous work [30]. In this paper, for simple demonstration of working principle, the experiment is performed using the A0 and S0 modes, due to their better quality factors of frequency signals and relatively more stable signals.

5.2 Temperature sensitivity

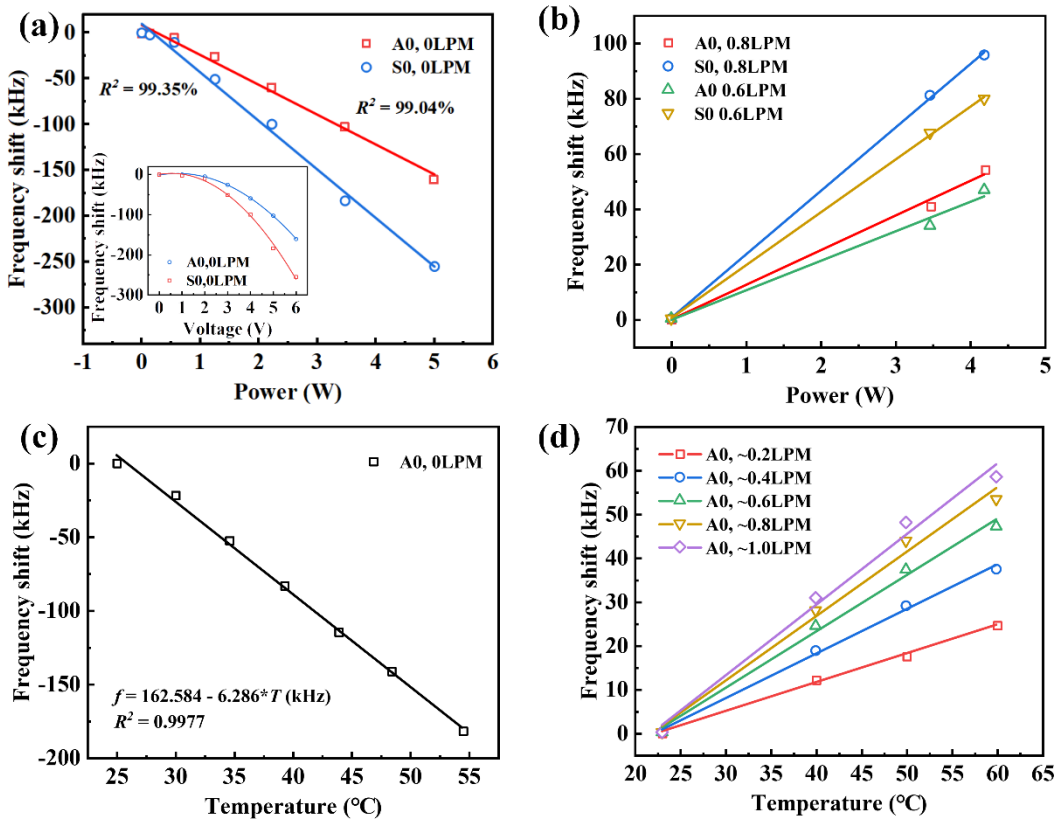

Fig. 5. Fitted line plot of frequency shift changing with heating power in the absence (a) and presence (b) of airflow. Fitted line plot of frequency shift changing with heating temperature in the absence (c) and presence (d) of airflow.

When there is no airflow, the frequency shift shows a good linearity with the power of heat source, but shows a quadratic relationship with the voltage of heat source, as shown in Fig. 5a and the inset. Fig. 5b shows a linear relationship between the power of heat source and the frequency shift when the airflow is present. Similarly, Figs. 5c and 5d indicate linear relationships between the temperature of heat source and the frequency shift without and with airflow, respectively. The temperature of the heat source is linearly related to the frequency shift, and the flow rates are determined by the slope of the curves. This linear relationship proves the correctness of the theoretical model, i.e., the heat radiation power is negligible, and the equivalent thermal resistances (R, R_1, and R_2) do not change with temperature.

5.3 Flow rate sensitivity

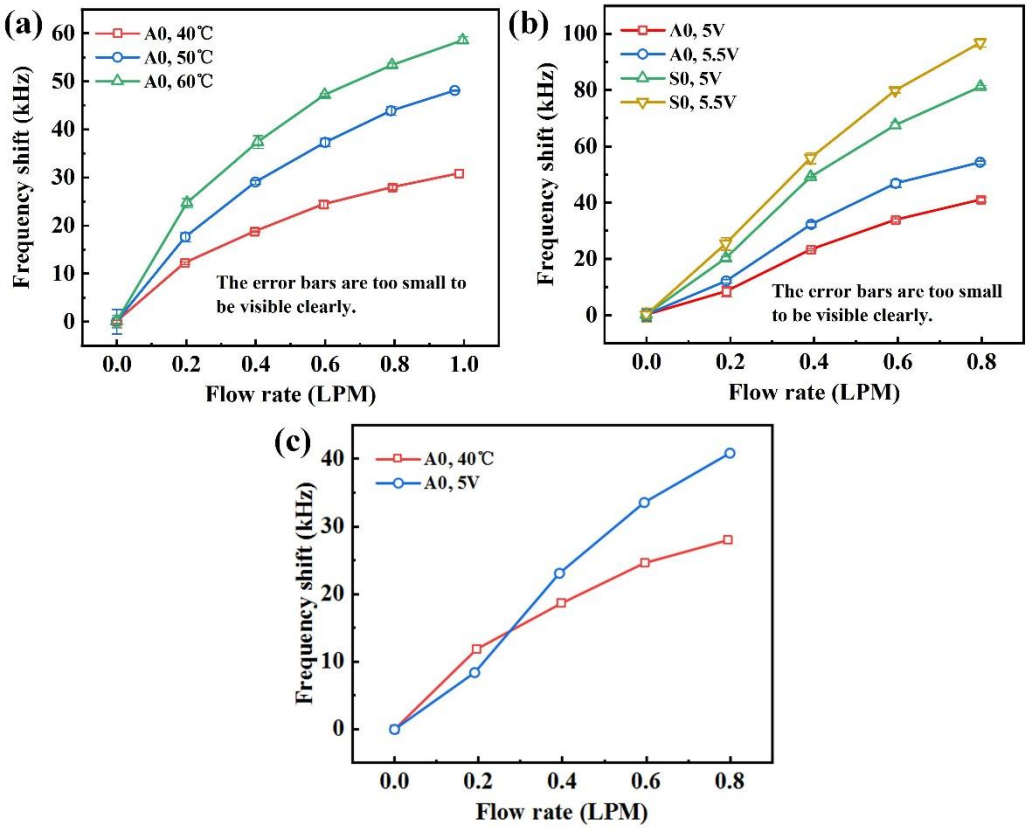

Fig. 6. (a) Frequency responses of the A0 mode to flow rate with CTHS of 40 °C, 50 °C and 60 °C. (b) Frequency responses of A0 and S0 mode to flow rate with CPHS of 5V and 5.5V. (c) Comparison of the sensitivities of CPHS mode and CTHS mode with almost identical initial temperature offset.

Fig. 6a shows the frequency responses at different temperatures of the heat source, i.e., 40 °C, 50 °C, and 60 °C. With a constant heating temperature, as the flow rate increases, the resonant frequency of the acoustic wave device increases and the sensitivity (i.e., the slope of the curve between frequency shift and flow rate) decreases. Moreover, a heat source with a higher temperature will result in a higher sensitivity. Fig. 6b demonstrates the frequency responses of A0 and S0 modes when the supply voltage of the heat source is 5 V (~3.47 W, initial temperature offset is ~15 °C) and 5.5 V (~4.20 W, initial temperature offset is ~21 °C), respectively. By comparing the responses of A0 and S0 modes at the same heating temperature and flow rate, it is found that a higher operating resonant frequency contributes to a larger frequency shift. The characteristics of the changing trend of these polylines are similar to those shown in Fig. 6a. With heat sources of a 40 °C CTHS and a 5V CPHS respectively, the initial temperature offsets are almost identical (~15 °C). But the flexible sensor with CPHS mode shows larger frequency shift (~40.86 kHz) than that with CTHS mode (28 kHz) when the flow rate is 0.8 LPM, which shows an increase rate of 46%., as shown in Fig. 6c.

Figs. 7a to 7c show the combined effects of flow rate and heating temperature/power on resonant frequency shifts of the flexible device. The resonant frequency shift is induced by heating power/temperature and gas flow, and either increase of heating power/temperature or increase of flow rate can increase the resonant frequency shift.

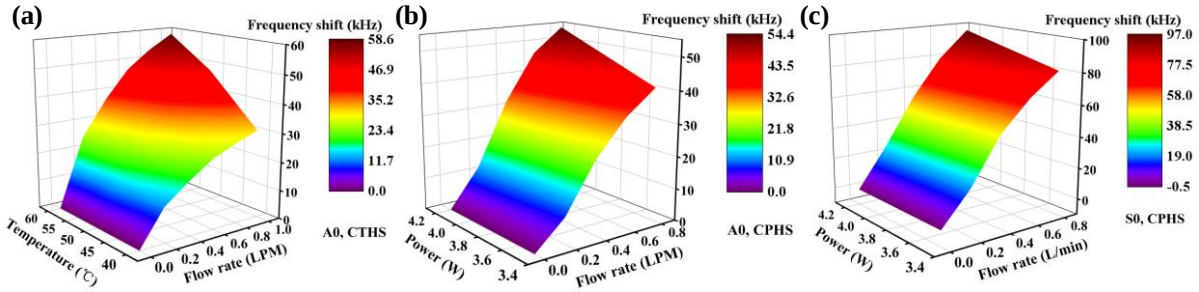

Fig. 7. Three-dimension plots of freqeuncy shifts of (a) A0, CTHS, (c) A0, CPHS and (c) S0, CPHS, where x = flow rate, y = heating power/temperature and z = resonant frequency shift.

5.4 Repeatability and response time

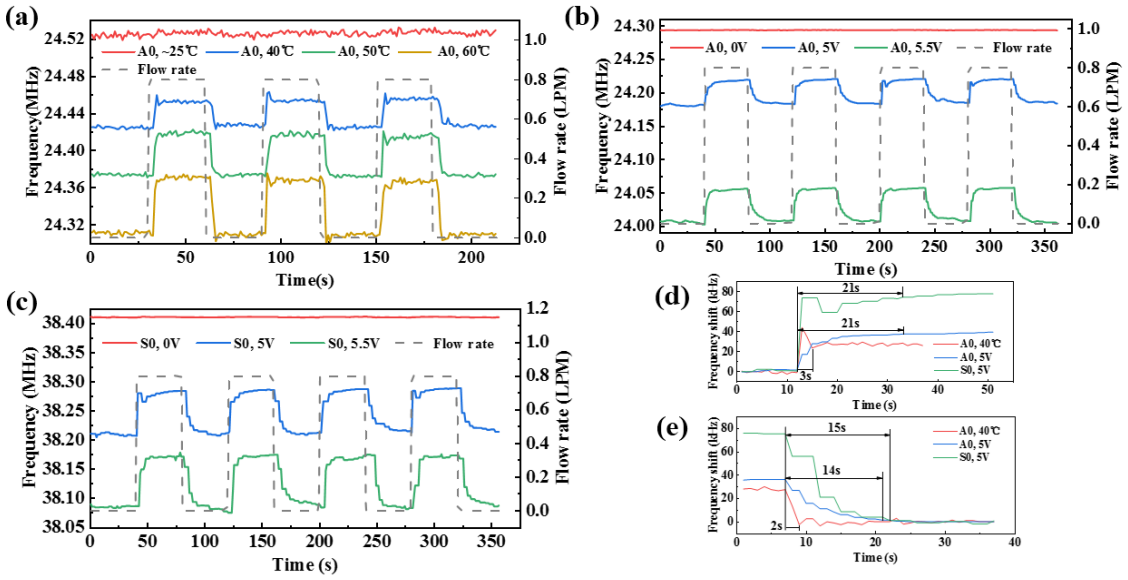

Fig. 8. Frequency responses to a cyclic flow rate between 0 and 0.8 LPM with (a) CTHS and A0 mode, (b) CPHS and A0 mode, (c) CPHS and S0 mode. Partial enlarged drawing of the processes of (d) increasing flow rate and (e) decreasing flow rate to reach new equilibrium states.

Fig. 8a demonstrates the variation of the resonant frequency when the flow rate is rapidly changed between 0 and 0.8 LPM at different heating temperatures. The flexible acoustic wave device shows both good repeatability and dynamic responses. Based on the flow changes shown in Fig. 8a, the shifts in resonant frequencies of A0 and S0 modes with a CPHS are shown in Figs. 8b and 8c, respectively. With the increase of heating temperature or power, the initial frequency shift is increased and consequently the sensitivity is increased. Without heating, changes of flow rate do not cause an apparent resonant frequency shift, as shown in red lines in Figs. 8a to 8c.

Figs. 8d and 8e compare the frequency shifts when increasing flow rate (decreasing substrate temperature and increasing resonant frequency) and decreasing flow rate (increasing substrate temperature and decreasing resonant frequency) to reach their new equilibrium states. Regardless of the heating process in Fig. 8d or the cooling process in Fig. 8e, the CTHS mode can significantly decrease the response time by about 7 times compared to the CPHS mode. The response time is defined as the time taken for the resonant frequency to reach 95% of the final steady value.

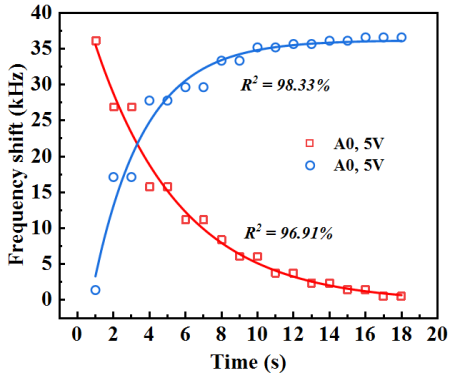

Fig. 9. Fitted line plot of frequency shift over time after changing flow rate between 0 and 0.8 LPM.

According to equations (8) and (9), a natural exponential function $F = a + be^{-t/\tau}$ is used to fit the data of transient frequency shift and time, where F is frequency shift, t is time, e is the nature constant, τ is the time constant, a and b are fitting parameters. The experimental data and part of fitting results are shown in Fig. 9, revealing an excellent agreement (R^2 = 98.33% and 96.91%), validating the theoretical model. The values of time constant τ of the transient responses obtained from Figs. 8d and 8e are listed in Table. 1. With the CTHS (A0, 40 °C), the flexible acoustic wave device shows significant advantage in terms of response times compared to those with the CPHS (A0, 5 V and S0, 5 V).

Table. 1. Time constants obtained by exponential fitting of the data in Figs. 8d and 8e

	Time constant, τ (s)	
	Increasing flow rate, Fig. 8d	Decreasing flow rate, Fig. 8e
A0, 40 °C	0.40	0.98
A0, 5 V	2.83	4.79
S0, 5 V	4.46	5.46

5.5 Hysteresis characteristics

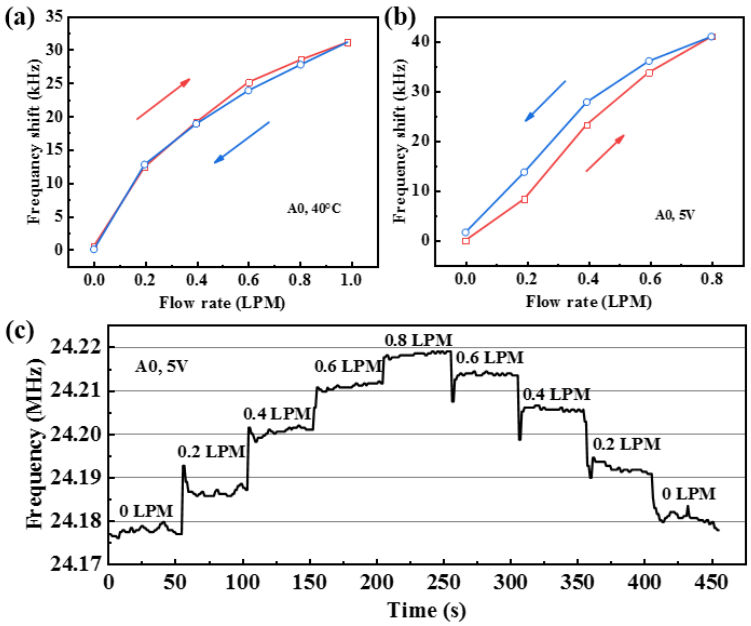

Fig. 10. A cyclic flow is applied for measuring the frequency hysteresis using (a) CTHS and (b) CPHS. (c) Frequency responses of the acoustic wave device when the flow rate increases from 0 to 0.8 LPM and then decreases from 0.8 to 0 LPM in step of 0.2 LPM.

In order to study the hysteresis characteristics during the transient response cycle, the device was first heated using a CTHS. The flow rate is increased from 0 to 1 LPM, and then decreased from 1 LPM to 0. During this process, the frequency shift is measured and recorded. As shown in Fig. 10a, the effect of hysteresis is nearly negligible. Fig. 10b shows the hysteresis effect when the device was heated by a CPHS with a flow rate cycling from 0 to 0.8 LPM. Obviously, the hysteresis effect in Fig. 10b is more significant compared to that in Fig. 10a. Fig. 10c shows the variation of the resonant frequency with time under the conditions defined in Fig. 10b. A commercial flow controller (Alicat MC-20SLPM-D) was used to calibrate the flow controller, and it was found that there is no hysteresis in flow rate at the steady state, and so there is no hysteresis in heat transfer coefficient h and the force exerted by airflow on the device. Therefore, the hysteresis is caused by the small gap between the CPHS and device.

5.6 Comparison with other rigid SAW flow sensors

Besides the flexible nature, our ZnO/Al based flexible sensor shows a significant advantage in response time compared with other rigid counterparts. As shown in Table. 2, the response speed is improved by at least 3.5 times (CPHS) and 25 times (CTHS) compared to the response time of ~75 s in [31]. On the other hand, due to the large TCF value of the flexible acoustic wave sensor, it can achieve a comparable relative sensitivity with a lower initial temperature offset (15°C - 35°C) than those of the rigid counterparts, e.g., lithium niobate based SAW sensors (56°C and 87°C) reported in [25] and [31]. This indicates that the flexible flow sensor has a higher relative sensitivity with identical initial temperature offset values. Compared with quartz-based SH-APM flow sensors reported in Ref. [32], the flexible acoustic wave flow sensor shows 5.8 times higher absolute sensitivity and 15 times higher relative sensitivity.

Table. 2. Comparisons of the characteristics of flexible acoustic wave device in this paper with those rigid SAW flow sensors reported in literature.

Acoustic wave type	Heating condition	Response time	Absolute sensitivity	Relative sensitivity	Ref.

Lamb	~81 °C	~90 s for 0.2 LPM	140 kHz for 1 LPM	1917.8 ppm for 1 LPM	[25]
Rayleigh	~112 °C	~75 s for 0.1 LPM	160 kHz for 1 LPM	2053.2 ppm for 1 LPM	[31]
Rayleigh	1.81 W	>200 s for 0.8 LPM	~3.5 kHz for 0.8 LPM	35.7 ppm for 0.8 LPM	[32]
SH-APM	2 W	>200 s for 0.7 LPM	~14 kHz for 0.7 LPM	140.4 ppm for 0.7 LPM	[32]
Dual-SAW	NA	>80 s for 0.3 LPM	~8 degree phase shift for 1 LPM	NA	[33]
Lamb	CTHS A0 mode 60 °C	~2 s for 0.8 LPM	53.4 kHz for 0.8 LPM	2176.8 ppm for 0.8 LPM	This work
	CPHS S0 mode ~42 °C	~21 s for 0.8 LPM	81 kHz for 0.8 LPM	2108.8 ppm for 0.8 LPM	
	CTHS A0 mode 40 °C	~3 s for 0.8 LPM	27.9 kHz for 0.8 LPM	1138.5 ppm for 0.8 LPM	

6. Conclusions

In this work, a flexible ZnO/Al acoustic wave device has been developed and demonstrated for the measurement of gas flow rate. Owing to its superior flexibility, the device can conform perfectly to the curved surfaces without interference in the original flow field. The flexible device shows the ability to work in both flat and bent/curved states. Bending the acoustic wave device will not introduce obvious deterioration to the flow rate measurement performance, e.g., increased noise. Experiment results in Fig. 8 show that the transient response of the resonant frequency is shifted over time, which follows the exponential relationship and is consistent with the theoretical analysis. Compared with other rigid counterparts, the flexible device shows a significant advantage in response time, improving the speed of response by at least 3.5 times (CPHS) and 25 times (CTHS). As the initial temperature offset increases, the sensitivity increases, while there is no significant difference in response time. The use of CPHS can increase the sensitivity but at the cost of longer response time. Due to the high TCF of the flexible acoustic wave sensor, it can achieve comparable relative sensitivity with lower initial temperature offset (15°C - 35°C) than other rigid counterparts (56 °C and 87 °C). Compared with that of A0 mode, the resonant frequency shift of the S0 mode is larger due to the higher resonant frequency, while the response time is almost the same. The frequency shift is negligible without initial temperature offset, indicating that the frequency response is mainly caused by thermal effects. The proposed flexible device exhibits high sensitivity and fast response with a great potential in flow rate measurements on curved surfaces.

Acknowledgement

This work is supported by the “National Natural Science Foundation of China (51875521)”, the “Zhejiang Provincial Natural Science Foundation of China (LZ19E050002)”, the “Science Fund for Creative Research Groups of National Natural Science Foundation of China (51821093)”, the UK Engineering and Physical Sciences Research Council (EPSRC) for support under grant EP/P018998/1, Newton Mobility Grant (IE161019) through Royal Society and the National Natural Science Foundation of China.

Reference

[1] Wang T, Guo Y, Wan P, Zhang H, Chen X and Sun X 2016 Flexible Transparent Electronic Gas Sensors *Small* **12** 3748–56

[2] Melzer M, Mönch J I, Makarov D, Zabila Y, Cañón Bermúdez G S, Karnaushenko D, Baunack S, Bahr F, Yan C, Kaltenbrunner M and Schmidt O G 2015 Wearable Magnetic Field Sensors for Flexible Electronics *Adv. Mater.* **27** 1274–80

[3] Kang H, Jung S, Jeong S, Kim G and Lee K 2015 Polymer-metal hybrid transparent electrodes for flexible electronics *Nat. Commun.* **6** 6503

[4] Sekitani T, Zschieschang U, Klauk H and Someya T 2010 Flexible organic transistors and circuits with extreme bending stability *Nat. Mater.* **9** 1015–22

[5] Shen W, Zhang X, Huang Q, Xu Q and Song W 2014 Preparation of solid silver nanoparticles for inkjet printed flexible electronics with high conductivity *Nanoscale* **6** 1622–8

[6] Lee S, Bae S-H, Lin L, Yang Y, Park C, Kim S-W, Cha S N, Kim H, Park Y J and Wang Z L 2013 Super-Flexible Nanogenerator for Energy Harvesting from Gentle Wind and as an Active Deformation Sensor *Adv. Funct. Mater.* **23** 2445–9

[7] Fu Y Q, Luo J K, Nguyen N T, Walton A J, Flewitt A J, Zu X T, Li Y, McHale G, Matthews A, Iborra E, Du H and Milne W I 2017 Advances in piezoelectric thin films for acoustic biosensors, acoustofluidics and lab-on-chip applications *Prog. Mater. Sci.* **89** 31–91
[8] Xuan W, He X, Chen J, Wang W, Wang X, Xu Y, Xu Z, Fu Y Q and Luo J K 2015 High sensitivity flexible Lamb-wave humidity sensors with a graphene oxide sensing layer *Nanoscale* **7** 7430–6
[9] Chen J, He X, Wang W, Xuan W, Zhou J, Wang X, Dong S R, Garner S, Cimo P and Luo J K 2014 Bendable transparent ZnO thin film surface acoustic wave strain sensors on ultra-thin flexible glass substrates *J. Mater. Chem. C* **2** 9109–14
[10] Xu H, Cao Z, Dong S, Chen J, Xuan W, Cheng W, Huang S, Shi L, Liu S, Farooq U, Qadir A and Luo J 2018 Flexible dual-mode surface acoustic wave strain sensor based on crystalline LiNbO3 thin film *J. Micromechanics Microengineering* **29** 25003
[11] Tao R, Hasan S A, Wang H Z, Zhou J, Luo J T, McHale G, Gibson D, Canyelles-Pericas P, Cooke M D, Wood D, Liu Y, Wu Q, Ng W P, Franke T and Fu Y Q 2018 Bimorph material/structure designs for high sensitivity flexible surface acoustic wave temperature sensors *Sci. Rep.* **8** 9052
[12] Tao X, Jin H, Mintken M, Wolff N, Wang Y, Tao R, Li Y, Torun H, Xie J, Luo J, Zhou J, Wu Q, Dong S, Luo J, Kienle L, Adelung R, Mishra Y K and Fu Y Q 2020 Three-Dimensional Tetrapodal ZnO Microstructured Network Based Flexible Surface Acoustic Wave Device for Ultraviolet and Respiration Monitoring Applications *ACS Appl. Nano Mater.* **3** 1468–78
[13] Liu Y, Li Y, el-Hady A M, Zhao C, Du J F, Liu Y and Fu Y Q 2015 Flexible and bendable acoustofluidics based on ZnO film coated aluminium foil *Sensors Actuators B Chem.* **221** 230–5
[14] Tao R, McHale G, Reboud J, Cooper J M, Torun H, Luo J, Luo J, Yang X, Zhou J, Canyelles-Pericas P, Wu Q and Fu Y 2020 Hierarchical Nanotexturing Enables Acoustofluidics on Slippery yet Sticky, Flexible Surfaces *Nano Lett.* **20** 3263–70
[15] Tao R, Reboud J, Torun H, McHale G, Dodd L E, Wu Q, Tao K, Yang X, Luo J T, Todryk S and Fu Y 2020 Integrating microfluidics and biosensing on a single flexible acoustic device using hybrid modes *Lab Chip* **20** 1002–11
[16] Ejeian F, Azadi S, Razmjou A, Orooji Y, Kottapalli A, Ebrahimi Warkiani M and Asadnia M 2019 Design and applications of MEMS flow sensors: A review *Sensors Actuators A Phys.* **295** 483–502
[17] Gardner E L W, Vincent T A, Jones R G, Gardner J W, Coull J, Luca A De and Udrea F 2019 MEMS Thermal Flow Sensors— An Accuracy Investigation *IEEE Sens. J.* **19** 2991–8
[18] Balakrishnan V, Dinh T, Phan H-P, Dao D V and Nguyen N-T 2018 Highly sensitive 3C-SiC on glass based thermal flow sensor realized using MEMS technology *Sensors Actuators A Phys.* **279** 293–305
[19] Abbasnejad B, Thorby W, Razmjou A, Jin D, Asadnia M and Ebrahimi Warkiani M 2018 MEMS piezoresistive flow sensors for sleep apnea therapy *Sensors Actuators A Phys.* **279** 577–85
[20] Hoera C, Skadell M M, Pfeiffer S A, Pahl M, Shu Z, Beckert E and Belder D 2016 A chip-integrated highly variable thermal flow rate sensor *Sensors Actuators B Chem.* **225** 42–9
[21] Sharma P, Motte J-F, Fournel F, Cross B, Charlaix E and Picard C 2018 A Direct Sensor to Measure Minute Liquid Flow Rates *Nano Lett.* **18** 5726–30
[22] Bora M, Kottapalli A G P, Miao J M and Triantafyllou M S 2017 Fish-inspired self-powered microelectromechanical flow sensor with biomimetic hydrogel cupula *APL Mater.* **5** 104902
[23] Chen X, Xu J, Chen H, Ding H and Xie J 2019 High-Accuracy Ultrasonic Rangefinders via pMUTs Arrays Using Multi-Frequency Continuous Waves *J. Microelectromechanical Syst.* **28** 634–42
[24] Nguyen S D, Paprotny I, Wright P K and White R M 2015 MEMS capacitive flow sensor for natural gas pipelines *Sensors Actuators A Phys.* **231** 28–34
[25] Joshi S G 1991 Surface-Acoustic-Wave (SAW) Flow Sensor *IEEE Trans. Ultrason. Ferroelectr. Freq. Control* **38** 148–54
[26] Zhou L, Manceau J-F and Bastien F 2012 Interaction between gas flow and a Lamb waves based microsensor *Sensors Actuators A Phys.* **181** 1–5
[27] Weyburne D W 2006 A mathematical description of the fluid boundary layer *Appl. Math. Comput.* **175** 1675–84
[28] Zhang Q, Wang Y, Tao R, Li D, Fu Y and Xie J 2020 Flexible ZnO Thin Film Surface Acoustic Wave Device for Flow Rate Measurement *2020 IEEE 33rd International Conference on Micro Electro Mechanical Systems (MEMS)* pp 638–41
[29] Liu Y, Luo J T, Zhao C, Zhou J, Hasan S A, Li Y, Cooke M, Wu Q, Ng W P, Du J F, Yu Q, Liu Y and Fu Y Q 2016 Annealing Effect on Structural, Functional, and Device Properties of Flexible ZnO Acoustic Wave Sensors Based on Commercially Available Al Foil *IEEE Trans. Electron Devices* **63** 4535–41

[30] Tao R, Wang W B, Luo J T, Ahmad Hasan S, Torun H, Canyelles-Pericas P, Zhou J, Xuan W P, Cooke M D, Gibson D, Wu Q, Ng W P, Luo J K and Fu Y Q 2019 Thin film flexible/bendable acoustic wave devices: Evolution, hybridization and decoupling of multiple acoustic wave modes *Surf. Coatings Technol.* **357** 587–94

[31] Joshi S G 1989 Use of a Surface-Acoustic-Wave (SAW) Device to Measure Gas Flow *IEEE Trans. Instrum. Meas.* **38** 824–6

[32] Rebière D, Déjous C, Pistré J, Aucouturier J L, Tiret C and Planade R 1994 Acoustic wave devices to measure gas flow: Comparison between surface acoustic wave (SAW) and shear horizontal acoustic plate mode (SH-APM) oscillators *Sensors Actuators A. Phys.* **42** 384–8

[33] Nomura T, Saitoh A and Koyama K 2007 Mass Flow Sensor Using Dual SAW Device *2007 IEEE International Frequency Control Symposium Joint with the 21st European Frequency and Time Forum* pp 25–30